

Interferences in the $3p^4nl$ satellite emission following the excitation of argon across the $2p_{1/2}^54s$ and $2p_{3/2}^53d J=1$ resonances

S. Fritzsche*

Institut für Physik, Universität Kassel, D-34132 Kassel, Germany

J. Nikkinen, S.-M. Huttula, H. Aksela, M. Huttula, and S. Aksela

Department of Physical Sciences, University of Oulu, P.O. Box 3000, FIN-90014, University of Oulu, Finland

(Received 6 July 2006; published 2 January 2007)

The intensity and angular distribution of the argon $3p^4nl$ photoelectron lines have been measured with a high resolution (of about 55 meV) in the 246.51–246.93 eV photon energy region. For these photon energies, the excitation of the $2p_{1/2}^54s$ and $2p_{3/2}^5(3d+5s) J=1$ intermediate resonances leads to a remarkable (interference) pattern in the intensity of the observed fine-structure states of the satellite lines, which can be attributed to a *coherent* interplay between the direct photoionization and various excitation-autoionization channels. Detailed computations show that this behavior in the observed electron intensities can be understood only if both the overlap of the resonances as well as their relative phases are taken into account. For these photon energies, therefore, any accurate description of the photoionization (with excitation) requires going beyond the two-step model, which separates the excitation process of the atoms from the subsequent photoelectron emission. Reasonable agreement between experiment and theory is found for most lines by applying multiconfiguration Dirac-Fock wave functions. Apart from a first quantitative analysis of the $3p^4nl$ electron lines, however, the high photon and electron energy resolution of the present experiments may stimulate future investigations on resonance phenomena in atomic photoionization, including rearrangement effects in the bound-state electron density and a refined treatment of the electron continuum.

DOI: [10.1103/PhysRevA.75.012501](https://doi.org/10.1103/PhysRevA.75.012501)

PACS number(s): 32.80.Dz, 32.80.Fb, 32.70.Fw, 32.70.Jz

I. INTRODUCTION

Resonances in atomic photoionization cross sections have been investigated for a long time as to the dependence on the frequency of the incoming light. Such resonances are of particular interest as they represent a clear signature that, besides that of the *direct* photoionization of one or several electrons by the radiation field, many-electron atoms and ions also possess an internal structure, which allows the electron emission to proceed along different “paths.” Owing to the quantum nature of atomic photoionization, of course, these paths in the excitation and decay of the atom *interfere* and hence, enable one to explore the electronic correlation in such systems. If, moreover, a sufficient high resolution is achieved, these interferences also lead to the formation of Fano profiles with either a constructive or destructive superposition of the quantum amplitudes [1].

A special type of these “resonances” in the photoionization cross sections are used also in the (so-called) resonant Auger spectroscopy. In this branch of spectroscopy, an inner-shell electron is first excited to some (unoccupied) valence shell, leading to a well-defined hole state of the atom or ion under consideration. In a second step, these hole states then autoionize, if embedded within the continuum of the next-higher charge state, completing thus the *photoionization* process. For an isolated resonance, this autoionization can be described quite independently of the creation process, i.e., within a two-step model. Recording, moreover, the spectra with much narrower bandwidth than the lifetime of the hole

state enables one to resolve the fine structure, which results from the coupling of the holes created in spectator Auger decay, together with the excited electron (the so-called Auger resonant Raman effect). After first measurements of resonant Auger spectra with subnatural linewidths [2,3], this method was applied widely also to the noble gas atoms, see e.g., Ref. [4] and references therein, and alkaline earth atoms [5] already at the time of second generation synchrotron radiation facilities, e.g., MAX-I.

With the increasing photon flux of the third generation synchrotron radiation facilities such as MAX-II, the recording of similar spectra as a function of photon energy became possible. The moderate resolution of the electron spectrometers, however, prevents one from resolving the fine structure of the Auger peaks, while the integrated intensity hardly displays hints of clear interference effects [6,7]. Detailed information about the energy dependence of individual final states becomes visible only in high-resolution electron spectra [8–10]. However, to avoid the drawbacks of the moderate electron-energy resolution, information about the intermediate resonances can be obtained by measuring the angular distribution and the polarization of the subsequent photon emission [11,12].

Argon and krypton are two particularly suitable examples for studying resonance phenomena in atomic systems. Despite their simple shell structure, namely, the excitation and decay of these atoms depend sensitively on many-electron effects, owing to the appearance of the nearly degenerate $3d$ and $4d$ subshells for argon and krypton, respectively. For both elements, moreover, a strong “coherence transfer” has been confirmed recently for several excitation and decay processes by studying, for instance, the angular distribution of

*Electronic address: s.fritzsche@physik.uni-kassel.de

the second-step Auger electron [13] or by analyzing the decay channels of “complete” experiments [14]. In this work, we report on the behavior of the argon $3p^4nl$ photoelectron lines as a function of the photon energy across the $2p_{1/2}^5 4s$ $J=1$ and $2p_{3/2}^5(3d+5s)$ $J=1$ photoabsorption resonances. These investigations extend a recent case study by Ricz *et al.* [15] who measured the angular distribution of the main $3p$ photoline in the 90–330 eV photon energy region. In that measurement, an enhancement of the line intensities due to the participator Auger decay via resonances could be resolved for the $3p_{1/2}$ and $3p_{3/2}$ photoelectron lines even with a moderate resolution of the spectrometer. Owing to a much higher electron-energy resolution—but by using about the same photon bandwidth of 50 meV—we are now able to analyze the intensity and angular distribution of the various $3p^4(3d+4s+5s)$ $J_f=1/2, \dots, 7/2$ satellite states if they are recorded with photon energies of ~ 246.5 eV, i.e., just *on top* and between the four $J=1$ intermediate resonances from above. Apart from the high-resolution measurements, emphasis was placed also on the theoretical analysis of the $3p^6 \rightarrow 3p^4(3d+4s+5s)$ photoionization with excitation process, which shows a quite different behavior for different final states of the photoion. Following a short account on the experiment in the next section, Sec. III then describes the photoionization *with* excitation as a unified process, which includes the overlap and interaction between the $2p_{1/2}^5 4s$ and $2p_{3/2}^5(3d+5s)$ resonances. Both the direct ionization as well as the resonant excitation with subsequent electron emission have been calculated by using multiconfiguration Dirac-Fock wave functions. Results and discussions are presented later in Sec. IV, while a few conclusions are given finally in Sec. V.

II. EXPERIMENT

Relative intensities and angular anisotropy parameters for transitions to the Ar $3p^4nl$ final states at the binding energy region $E_b=32$ –40 eV were measured as a function of photon energy across the closely spaced $2p_{1/2}^5 4s$ $J=1$ and $2p_{3/2}^5(3d+5s)$ $J=1$ photoabsorption resonances. Compared to the other $2p^5nl$ resonances, the $2p_{3/2}^5(3d+5s)$ $J=1$ resonance has the highest absorption strength whereas the $2p_{1/2}^5 4s$ $J=1$ resonance has the absorption strength of about 20% of the previous one. Both absorption peaks display a Lorentzian line shape due to the fact that the underlying direct valence photoionization cross sections are lower by several orders of magnitude.

The measurements were carried out at the gas phase beamline I411 at MAX-II storage ring in Lund, Sweden [16,17]. The ejected electrons were detected using the rotatable hemispherical SES-200 electron analyzer [18,19] with the kinetic-energy resolution of about 20 meV and the photon-energy resolution of about 50 meV. Since the used photon bandwidth is narrower than the inherent lifetime widths of the $2p_{1/2}^5 4s$ $J=1$ and $2p_{3/2}^5(3d+5s)$ $J=1$ resonances (109 and 125 meV [20], respectively) the line narrowing occurs in the photoelectron spectrum due to the Auger resonant Raman effect. The energies of $3p^4nl$ lines were calibrated using the Ar $3s$ photoelectron line whose binding energy

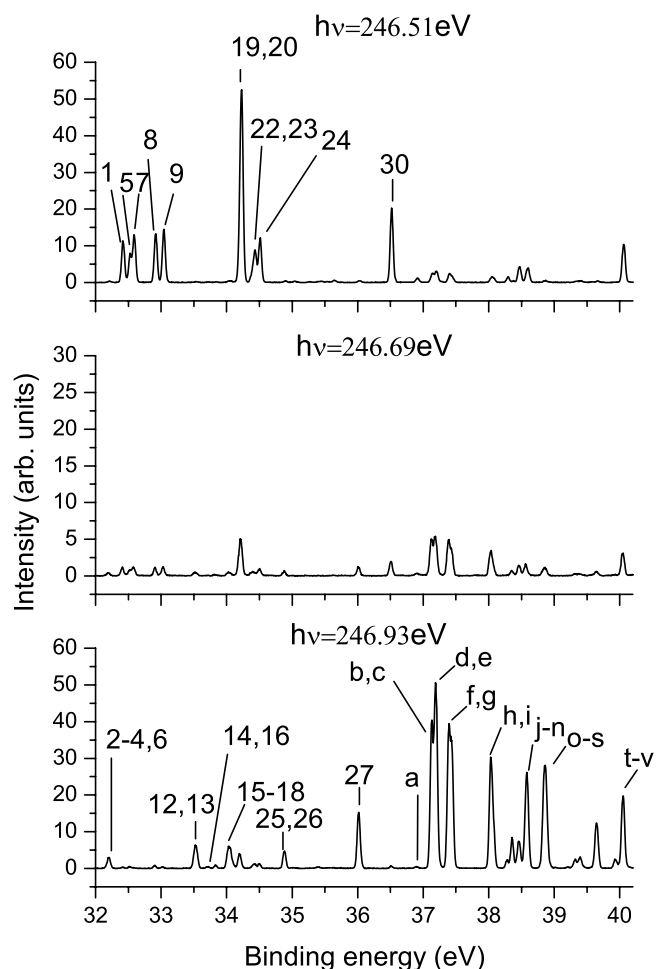


FIG. 1. Observed Ar $3p^4nl$ photoelectron spectrum at the angle of 54.7° and for three closely spaced photon energies: at the $2p_{1/2}^5 4s$ $J=1$ resonance (top panel: $h\nu=246.51$ eV), the $2p_{3/2}^5(3d+5s)$ $J=1$ resonances (bottom panel: $h\nu=246.93$ eV) and in between these resonances (middle panel: $h\nu=246.69$ eV).

$E_b=29.240$ eV is known from the literature [21].

In order to evaluate the relative intensities and angular anisotropy parameters of the $3p^4nl$ electron lines as a function of excitation energy, five different photon energies and three different angles of the electron analyzer with respect to the polarization direction of the incoming linearly polarized light were used in the measurements. The photon energies used were $h\nu=246.51$, 246.57, 246.69, 246.87, and 246.93 eV and the angles $\theta=0^\circ$, 54.7° , and 90° , respectively. While the first and the last of these excitation energies just coincide with the $2p_{1/2}^5 4s$ $J=1$ and $2p_{3/2}^5(3d+5s)$ $J=1$ resonance energies, the other three excitation energies lay in between the resonances. The transmission of the electron spectrometer of different angles was corrected with the aid of the known angular distribution parameters for a few well-resolved $3p^4nl$ electron lines. There was no need for the transmission correction in kinetic energy owing to the relatively short energy region and the high kinetic energies of the electrons. All measured spectra were least-squares fitted using the Voigt functions.

Figure 1 shows the $3s$ photoelectron spectrum at the bind-

ing energy region of the $3p^4nl$ satellite lines, measured at the angle of 54.7° . Spectra are shown for three photon energies at the $2p_{1/2}^5 4s J=1$ resonance [$h\nu=246.51$ eV (upper figure)], $2p_{3/2}^5(3d+5s) J=1$ resonance [$h\nu=246.93$ eV (lower figure)] and in between the resonances at $h\nu=246.69$ eV. This energy region includes the transitions to the $3p^4 4s$, $3p^4 3d$, and $3p^4 5s$ final states. Obviously, the low binding-energy area is due to transitions to the $3p^4 4s^{2S+1}L_{j_f}$ levels whereas the high binding-energy side is due to the transitions to the $3p^4 3d$ and $3p^4 5s^{2S+1}L_{j_f}$ final states. This assignment is also confirmed by optical data as known from Moore's tables [21]. The much higher photon and energy resolution, when compared to all previous case studies [22,23], enables us now to determine the fine structure of the electron spectrum in more detail.

III. THEORY AND COMPUTATIONS

A. Resonant photoionization

As mentioned above, the resonant photoionization with excitation is known also as the *resonant Auger effect* in the literature [4]. More often than not, this ionization process has been described as a two-step process in which an atom or ion in some initial state $|i\rangle$ is first excited into the resonant state $|m\rangle$ which, in a second step, then autoionizes under the emission of an electron, leading to a final ionic state $|f\rangle$. In this somehow simplified model of the resonant electron emission, therefore, each photoline in the observed spectrum is assumed to be populated only via a single resonance $|m\rangle$, which is well isolated from other resonances, and for which no overlap occurs. Obviously, however, this model becomes inappropriate if two or more resonances appear close in energy (when compared to their total widths) or if they obey a strong configuration mixing. If the direct photoionization from state $|i\rangle \rightarrow |f\rangle$ is negligible, the two-step model can still be applied but has then to be combined with the density matrix theory in order to allow coherence transfer through several steps of the photoexcitation and/or the subsequent Auger decay [24]. In practice, the two-step model is *preserved* in the formalism by replacing the single resonance $|m\rangle$ by a proper choice of the intermediate-state density matrix $\hat{\rho}_m$. During recent years, this theory has been applied very successfully to analyze the resonant $^1S_0 \rightarrow ^{1,3}P_1$ photoexcitation for various noble gases, including one or several steps in their subsequent Auger emission [25].

For studying the resonant photoionization *across* the resonances, i.e., as a function of the photon energy, the two-step model has to be replaced (or at least augmented properly) by a more rigorous treatment of the (dipole) photoionization amplitude

$$\begin{aligned}
 & D(\omega; \gamma_f J_f P_f, \epsilon \kappa_c; \gamma_i J_i P_i) \\
 &= \langle \gamma_f J_f P_f, \epsilon \kappa_c; J_i P_i | \mathcal{D}(\omega) | \gamma_i J_i P_i \rangle + \sum_m \\
 & \times \frac{\langle \gamma_f J_f P_f, \epsilon \kappa_c; J_i P_i | H - E_m | \gamma_m J_m P_m \rangle \langle \gamma_m J_m P_m | \mathcal{D} | \gamma_i J_i P_i \rangle}{E_i + \omega - E_m + i\Gamma_m/2},
 \end{aligned} \tag{1}$$

which connects the initial state $|\psi_i\rangle \equiv |\psi(\gamma_i J_i P_i)\rangle$ either directly (first term) or via one or several resonances $|\psi_m\rangle \equiv |\psi(\gamma_m J_m P_m)\rangle$ with some particular final state $|\psi(\gamma_f J_f P_f)\rangle$ of the photoion and the photoelectron in the continuum. In this notation of the resonant electron emission, we assume the photoelectron to escape by means of the partial wave $|\epsilon \kappa_c\rangle$ with kinetic energy $\epsilon = E_i + \omega - E_f$ and with well-defined angular momentum and parity. The “photoion+electron” then gives rise to the (total) final state $|\psi_f\rangle \equiv |\gamma_f J_f P_f, \epsilon \kappa_c; \gamma_i J_i P_i\rangle$ with total energy $E_f = E_i + \omega$, after the photon has been absorbed by the atom. As appropriate for a relativistic description of the bound-state electron density and the outgoing photoelectron, here we make use of the relativistic angular momentum quantum number

$$\kappa = \pm(j + 1/2) \quad \text{for } l = j \pm 1/2,$$

in order to denote the symmetry properties of the outgoing electron, i.e., its angular momentum j and parity $(-1)^l$. In Eq. (1), moreover, $\mathcal{D}(\omega)$ denotes the dipole operator (of the multielectron atom) and

$$\Gamma_m = \hbar \left(\sum_j A_a(m \rightarrow j) + \sum_{f'} A_r(d \rightarrow f') \right)^{-1}, \tag{2}$$

the total widths of the resonance state $|m\rangle$ which, in first-order perturbation theory, is given by the sum over all the individual Auger A_a and radiative rates A_r (widths) of the intermediate state $|m\rangle$. Apart from a possible direct photoionization amplitude (i.e., the first term in Eq. (1); for details see Ref. [26]), formula (1) therefore contains also the photoexcitation and autoionization amplitudes. Although all of these amplitudes are basically energy independent, at least if taken across or nearby some given resonance, the summation (second term) over the various resonances m may lead to either a constructive or destructive interference pattern in practically all observables, owing to the energy-dependent nominator and the moduli and relative phases of the amplitudes. In fact, the phases of the excitation-autoionization channels are mainly responsible for the extent to which a *coherence transfer* can be observed eventually in the resonant photoionization process.

As usual, the dipole amplitudes (1) are the *building blocks* for calculating the intensities and angular distribution parameters in the resonant photoionization of atoms and ions; from these amplitudes the cross section (intensity) for the photoelectron emission

$$\sigma = \frac{4\pi^2 \alpha \omega}{3(2J_i + 1)} \sum_{\kappa_c, J_i} |D(\omega; \gamma_f J_f P_f, \epsilon \kappa_c; \gamma_i J_i P_i)|^2 \tag{3}$$

is obtained by taking the sum over all the possible scattering states of the final system: photoion+electron. Obviously, this includes the summation over the partial waves of the photoelectron as well as the total angular momenta and parities $J_i^{P_i}$. Moreover, the angular parameter β [in the standard formula $W(\theta) \sim (1 + \beta P_2(\cos \theta))$] is described by some proper summation of these amplitudes

$$\beta = -\sqrt{\frac{10}{3}}\beta_{022}. \quad (4)$$

For linear polarized light, an explicit expression for the angular coefficients $\beta_{k_{\alpha}k_{\beta}k_{\gamma}}$ were displayed by Baier *et al.* [27], Eqs. (13) and (17), and need not be discussed here in further detail. Owing to the denominator in the second term of formula (1), both the intensity and the angular distribution of the emitted photoelectrons are expected to show a—more or less—pronounced resonance behavior. In addition, since the amplitudes (1) connect the initial state $|i\rangle$ with the final state $|f\rangle$ of the photoion (and with the photoelectron $|\epsilon\kappa_c\rangle$ in the continuum, having all a well-defined angular momentum and parity), the same dipole amplitudes also determine the alignment and orientation of the photoion as well as, if allowed energetically, its subsequent photon or electron emission [14].

Unfortunately, the computation of the dipole amplitudes (1) is hampered by the fact that the initial, intermediate, and final-ionic states have a quite different electronic structure, apart from the occupation of the various shells as indicated by the electron configuration. These differences are seen most easily from the radial extent of the one-electron functions in the representation of the wave functions, which are not quite orthogonal for the different atomic states. A rather remarkable *contraction* of the radial functions is found, in particular, for the $3p$, $3d$, as well as $4s$ orbitals, if an additional $2p$ hole occurs in the electron core of the atom. This *nonorthogonality* of the one-electron orbital functions is important especially for estimating the contribution from the direct photoionization, a computational issue to which we shall return in Sec. II C. Of similar importance, moreover, is the relative position and the widths of the resonances that we have adopted below from experiment. To understand the computation of the dipole amplitudes (1) in more detail, we shall first explain how the atomic states were generated and utilized in the evaluation of the various many-electron amplitudes in this formula.

B. Generation of wave functions

In the resonant photoexcitation of inner-shell electrons, at least the intermediate states $|m\rangle$ usually refer to highly correlated (many-electron) states, embedded energetically in the continuum of the photoion. For these resonances, therefore, special care has to be taken to calculate the photoexcitation and autoionization amplitudes. To describe the wave functions of free atoms (and ions), the multiconfiguration Dirac-Fock (MCDF) method has been found a versatile tool for the computation of many-electron energies and decay properties, especially if inner-shell electrons or several open shells are involved in the computations [28,29]. In this method, an atomic state is approximated by a linear combination of (so-called) configuration state functions (CSF) of the same symmetry

$$\psi_{\alpha}(PJ) = \sum_{r=1}^{n_c} c_r(\alpha) |\gamma_r PJ\rangle, \quad (5)$$

where n_c is the number of CSF and $\{c_r(\alpha)\}$ denotes the representation of the atomic state in this many-electron basis. In

most standard computations, the CSF are constructed as antisymmetrized products of a common set of orthonormal orbitals and are optimized on the basis of the Dirac-Coulomb Hamiltonian. Further relativistic contributions to the representation $\{c_r(\alpha)\}$ of the atomic states could be added but were found to play a rather negligible role for argon (ions) as considered in the present analysis.

Applying ansatz (5) for atomic states of interest, of course, both the dipole excitation and photoionization as well as the Auger amplitudes are traced back always to the computation of the corresponding interaction matrix within the given CSF basis. To this end, the wave functions from the well-known GRASP92 code [30] have been utilized within the RATIP program [31] in order to evaluate all the amplitudes as indicated above. In particular, this code allows one to include all the dominant effects from relativity and correlations within the same computational framework. Since the main features of the RATIP program have been discussed in Refs. [31,32], we need not recall them here in detail.

C. Direct photoionization cross sections

The interaction of atoms with light may lead to a (photo-)electron emission if the energy of the incident photon exceeds the ionization threshold. For wavelengths $\lambda_{ph} \gg r_{atom}$, i.e., if the electric-dipole ($E1$) approximation is appropriate, the absorbed photon always transfers an angular momentum $L=1$ and results in a change in the parity of the overall system photoion+electron. In most cases, hereby the photoion will be left in a final *hole* state where just one of the electrons is removed from the (electronic) configuration of the initial state $|\psi_i\rangle$. Much less likely, in contrast, is the formation of a final state $|f\rangle$ of the photoion, which is associated with an excitation of one *additional* electron as in the $3s^3 3p^6 \rightarrow 3s^2 3p^4 (3d+4s+5s)^{2S+1} L_{J_f}$ resonant photoionization. Such an ionization with excitation requires a *correlated* motion of the electrons, and its photoionization amplitude becomes nonzero only in second-order perturbation theory (i.e., if the electron-electron interaction is taken into account by an additional order in the perturbation expansion).

In the MCDF approximation, at least the size of these second-order amplitudes can be estimated, if the initial and final-ionic states are optimized independently, leading to (two sets of) electron orbitals, which are not quite orthogonal to each other. In this case, a nonzero amplitude may arise for this second-order process already in *first* order, if the overlap of all the one-electron orbitals is treated properly in the evaluation of the photoionization amplitudes [first term in Eq. (1)]. To estimate this direct part of the photoionization amplitudes, here we applied the recently implemented component PHOTO of the RATIP program. In practice, however, the direct photoionization cross sections were found $\sigma_{dir} < 10^{-2}$ b and hence, these amplitudes play a negligible role for the present discussion. Such relaxation effects were found important for the photoionization of inner-shell electrons for which the cross sections can be modified by up to 30% or even more [33].

D. Photoexcitation amplitudes

From the viewpoint of the (two-step) excitation-autoionization process of formula (1), the photoexcitation

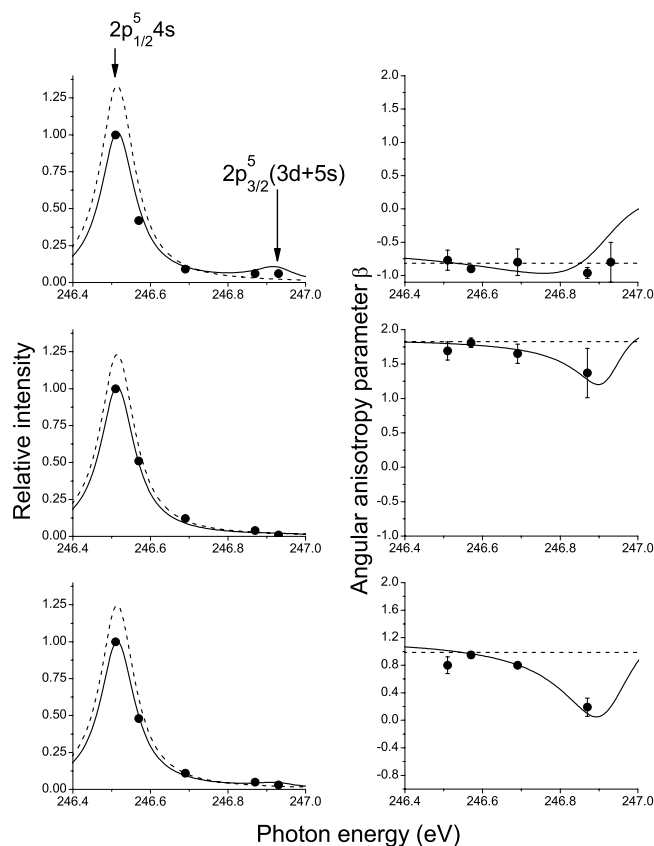


FIG. 2. Relative intensity (left) and angular anisotropy parameter β (right) of the photoelectron as a function of the photon energy ($h\nu$) in the region of the $2p_{1/2}^5 4s$ and $2p_{3/2}^5 (3d+5s)$ $J=1$ resonances. Results are shown for the resonant photoionization of argon into the fine-structure level $3p^4(^3P)4s^4P_{3/2}$ (upper set: final level 5 in Table II) and for the level $3p^4(^3P)4s^4P_{1/2}$ (middle set: level 7). In the lower part of the figure, the data are averaged for the two fine-structure levels. Experimental data (dots) are displayed and compared with two theoretical approximations A (dashed line) and B (solid line) for the representation of the bound-state wave functions. See the text for further details.

amplitudes $\langle \gamma_m J_m P_m | D | \gamma_i J_i P_i \rangle$ determine the relative population of the intermediate resonances $|m\rangle$, which (subsequently) autoionize to the final states $|f\rangle$. These photoabsorption amplitudes are closely related to the computation of transition probabilities and have been discussed in much detail in the literature [28]. Moreover, since these amplitudes connect two discrete states of the initial atom, their phase is

determined entirely by the coupling of the electrons in the initial and intermediate states but does not depend on the photon energy. In the RATIP program [31], these excitation amplitudes can be calculated by means of the REOS component [34] including, if appropriate, the rearrangement of the electron density in going from the initial state $|i\rangle$ to one of the resonances $|m\rangle$.

E. Auger amplitudes

Similarly to the photoionization of the initial atom, the calculation of the Auger amplitudes in Eq. (1) requires the coupling of the bound-state electrons in the resonant state $|m\rangle$ to the electron continuum. This coupling is caused mainly by the interaction among the bound-state electrons but might be affected also by the configuration mixing between different autoionization channels in the course of the emission process, i.e., by the so-called interchannel interactions. Apart from a very few case studies on the K - LL and K - LM spectra of noble gases [35,36], however, it has become common practice during the last decade to neglect both the interchannel interactions as well as the nonorthogonality in the evaluation of the many-electron amplitudes. The assumption of a common set of *orthonormal* orbitals for the intermediate and final states of the photoion means that the transition operator $H-E_m$ (which contains, besides the atomic Hamiltonian H , the total energy E_m of the intermediate state $|m\rangle$) can be replaced by the electron-electron interaction, $H-E_m \approx V_0$. For light and medium elements, moreover, it is typically sufficient to include the instantaneous Coulomb repulsion between the electrons, $V = \sum_{i<j} 1/|\vec{r}_i - \vec{r}_j|$, but to omit the Breit contributions, which are important for highly charged ions [37]. Indeed, the restriction to the electron-electron interaction in the computation (evaluation) of the Auger amplitudes is standard in all presently available Auger codes, even if the orbital functions of the resonant state $|m\rangle$ and the final-ionic state $|f\rangle$ are not taken orthogonal to each other. This treatment has been implemented therefore also in the Auger component of the RATIP program, in which the continuum spinors are solved within a spherical but level-dependent potential of the final ion (the so-called *optimal level* scheme in the GRASP92 program); this scheme also includes the exchange interaction of the emitted electron with the bound-state density. Often, the number of possible scattering states $|\gamma_f J_f P_f, \epsilon \kappa_c; \gamma_i J_i P_i\rangle$ of a system increases rapidly as the free electrons may couple in quite different ways to the bound-state electrons. For further details on the com-

TABLE I. Excitation energies, widths, and leading contributions in the LSJ coupling of the $2p_{1/2}^5 4s$ and $2p_{3/2}^5 (3d+5s)$ $J=1$ intermediate resonances.

Resonance	Excitation energy (eV)		Widths (meV)		Leading contributions (This calculation)
	Experiment [38]	This calculation	Experiment [20]	This calculation	
$2p_{1/2}^5 4s$	246.514(4)	246.556	109 ± 3	125.9	63.5% of $2p^5 4s ({}^2P)^3 P + 34.2\%$ of $2p^5 4s ({}^2P)^1 P$
$2p_{1/2}^5 5s$		246.628		126.6	65.6% of $2p^5 5s ({}^2P)^1 P + 31.9\%$ of $2p^5 5s ({}^2P)^3 P$
$2p_{1/2}^5 3d$	246.927(1)	246.652	125 ± 3	126.4	83.5% of $2p^5 3d ({}^2P)^3 P + 11.5\%$ of $2p^5 3d ({}^2P)^3 D$
$2p_{1/2}^5 3d$		246.677		126.8	61.3% of $2p^5 3d ({}^2P)^1 P + 38.3\%$ of $2p^5 3d ({}^2P)^3 D$

TABLE II. Excitation energies and leading contributions in a LS -coupled basis for the representation of the 30 lowest (satellite) states from the final $3p^4(3d+4s+4d+5s+5d+6s+7s)$ spectator configurations. The excitation energies (in eV) of these $^{2S+1}L_{J_f}$ final states are taken with respect to the $3p^6\ ^1S_0$ ground state of the neutral argon.

No.	Final state	J_f	Energy (eV)		Leading contributions (This calculation)
			Experiment [23]	This calculation	
1	$3p^44s$	5/2	32.404	30.56	93.4% of $4s(^3P)^4P+4.5%$ of $5s(^3P)^4P$
2	$3p^43d$	7/2	32.166	30.62	54.3% of $3d(^3P)^4D+44.2%$ of $4d(^3P)^4D$
3	$3p^43d$	5/2	32.185	30.64	14.0% of $3d(^3P)^2F+13.0%$ of $3d(^3P)^4D+11.0%$ of $4d(^3P)^4D$
4	$3p^43d$	3/2	32.204	30.66	20.2% of $4s(^3P)^4P+18.0%$ of $3d(^3P)^4D+17.0%$ of $4d(^3P)^4D$
5	$3p^44s$	3/2	32.508	30.67	72.3% of $4s(^3P)^4P+4.4%$ of $4d(^3P)^4D$
6	$3p^43d$	1/2	32.217	30.68	48.1% of $3d(^3P)^4D+41.6%$ of $4d(^3P)^4D$
7	$3p^44s$	1/2	32.572	30.74	86.1% of $4s(^3P)^2P+7.2%$ of $4s(^3P)^4P$
8	$3p^44s$	3/2	32.900	31.10	94.6% of $4s(^3P)^2P$
9	$3p^44s$	1/2	33.026	31.23	88.2% of $4s(^3P)^4P+7.5%$ of $4s(^3P)^2P$
10	$3p^43d$	9/2		31.84	51.0% of $3d(^3P)^4F+48.6%$ of $4d(^3P)^4F$
11	$3p^43d$	7/2		31.91	52.8% of $3d(^3P)^4F+43.5%$ of $4d(^3P)^4F$
12	$3p^43d$	5/2	33.503	31.96	19.1% of $3d(^3P)^4F+13.4%$ of $3d(^3P)^2F+11.2%$ of $4d(^3P)^4F$
13	$3p^43d$	3/2	33.536	32.00	17.6% of $3d(^3P)^2D+17.5%$ of $3d(^3P)^2P+16.4%$ of $3d(^3P)^4D$
14	$3p^43d$	1/2	33.702	32.53	28.6% of $3d(^3P)^4P+15.6%$ of $3d(^3P)^2P+15.3%$ of $4d(^3P)^4P$
15	$3p^43d$	1/2	34.014	32.57	30.6% of $3d(^3P)^4P+18.7%$ of $4d(^3P)^4P+14.4%$ of $3d(^3P)^2P$
16	$3p^43d$	3/2	33.821	32.57	42.8% of $3d(^3P)^4P+26.6%$ of $4d(^3P)^4P+7.8%$ of $3d(^3P)^4F$
17	$3p^43d$	5/2		32.63	19.4% of $3d(^3P)^4P+13.9%$ of $4d(^3P)^4P+12.0%$ of $3d(^3P)^2F$
18	$3p^44d$	3/2	34.048	32.68	15.8% of $4d(^1D)^2P+14.8%$ of $3d(^3P)^2P+14.5%$ of $3d(^1D)^2P$
19	$3p^44s$	3/2	34.186	32.72	56.8% of $4s(^1D)^2D+5.8%$ of $3d(^3P)^4F+5.6%$ of $4d(^1D)^2P$
20	$3p^44s$	5/2	34.214	32.73	76.8% of $4s(^1D)^2D+5.3%$ of $3d(^1D)^2D+4.8%$ of $4d(^1D)^2D$
21	$3p^43d$	7/2		32.89	59.8% of $3d(^3P)^2F+31.9%$ of $4d(^3P)^2F$
22	$3p^43d$	5/2	34.376	33.01	14.5% of $3d(^3P)^2F+14.4%$ of $3d(^3P)^4D+11.9%$ of $3d(^3P)^4D$
23	$3p^44s$	3/2	34.416	33.22	24.5% of $4s(^1D)^2D+16.0%$ of $3d(^1D)^2D+14.8%$ of $4d(^1D)^2D$
24	$3p^44d$	5/2	34.492	33.30	18.9% of $4d(^1D)^2D+17.4%$ of $4s(^1D)^2D+17.3%$ of $3d(^3P)^2D$
25	$3p^43d$	9/2	34.876	33.72	50.3% of $3d(^1D)^2G+49.3%$ of $4d(^1D)^2G$
26	$3p^43d$	7/2	34.879	33.72	54.1% of $3d(^1D)^2G+37.7%$ of $4d(^1D)^2G+6.7%$ of $5d(^1D)^2G$
27	$3p^43d$	5/2	36.006	34.97	59.9% of $3d(^1D)^2F+30.6%$ of $4d(^1D)^2F$
28	$3p^43d$	7/2		34.99	56.8% of $3d(^1D)^2F+35.9%$ of $4d(^1D)^2F+6.4%$ of $3d(^3P)^2F$
29	$3p^43d$	5/2		35.72	44.5% of $3d(^3P)^2D+21.6%$ of $3d(^1D)^2D+7.2%$ of $4d(^1D)^2D$
30	$3p^44s$	1/2	36.504	35.76	90.3% of $4s(^1S)^2S+4.1%$ of $3d(^1D)^2S$

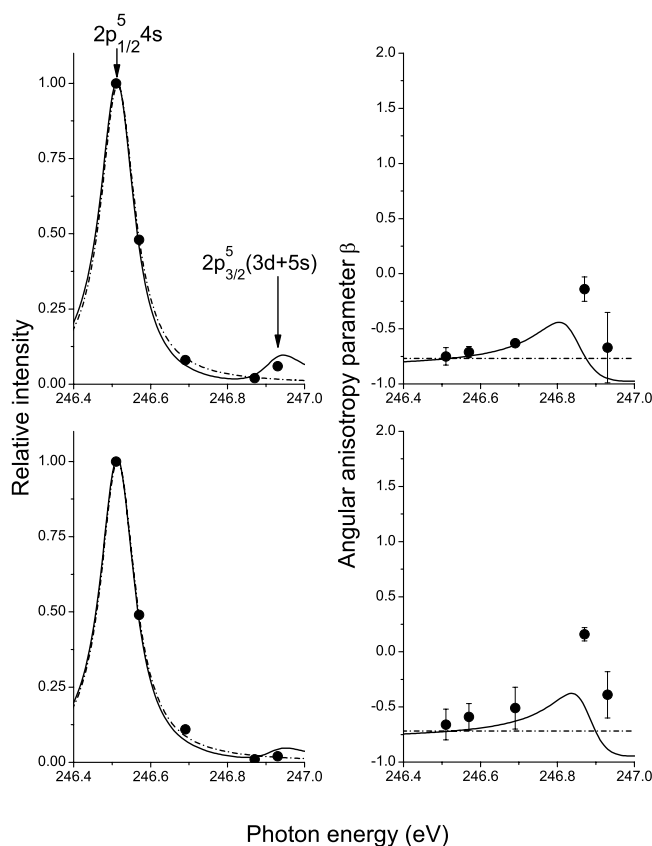


FIG. 3. Same as Fig. 2 but results are shown here for the resonant photoionization of argon into the $3p^4(^3P)4s^2P_{1/2,3/2}$ fine-structure levels, which correspond to level 8 (upper set) and level 9 (lower set) in Table II, respectively. Calculations including all the four $J=1$ resonances incorporated (solid line) are compared with those including only the $2p_{1/2}^5 4s J=1$ resonance (dashed line) in formula (1). All these computations here have been carried out by using our “best” representation of the atomic bound states.

putations of the Auger matrix elements and relative intensities, we refer the reader to Refs. [29,35].

With the discussion of the Auger amplitudes in Eq. (1), we now have all the ingredients available in order to calculate the full (dipole) amplitudes for the photoionization with excitation, starting from the ground state of the (argon) atoms. The energies and width of the individual resonance states $|m\rangle$ in this formula can be calculated with an accuracy that is sufficient for the *identification* of all the resonances involved. For a quantitative analysis of such high-resolution experiments, however, these energies and widths were better taken from previous measurements in order to facilitate a direct comparison between experiment and theory for the relative intensities and angular anisotropy parameters across the resonances from above. In the next section, formulas (1)–(3) are applied to the $3p^6 1S_0 \rightarrow 3p^4(3d+4s+5s)$ satellites of the $3s$ photoionization of argon in the region of the four $2p_{1/2}^5 4s$ and $2p_{3/2}^5(3d+5s) J=1$ resonances.

IV. RESULTS AND DISCUSSION

A. $2p_{1/2}^5 4s$ and $2p_{3/2}^5(3d+5s)$ resonances

At photon energies of about $\hbar\omega \sim 246$ eV, the photoexcitation of argon leads to either a $2p_{1/2}$ or $2p_{3/2}$ hole state as

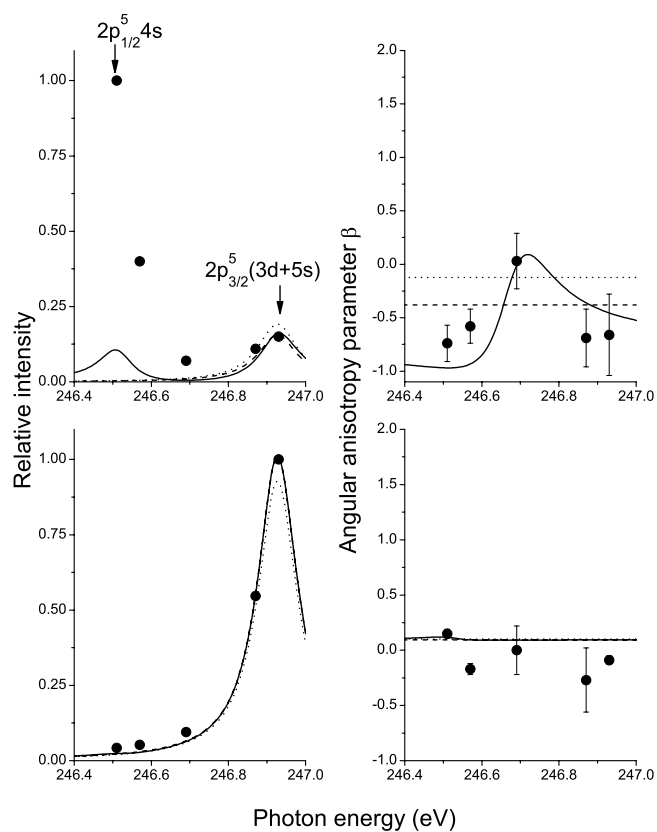


FIG. 4. Same as Fig. 2 but the results are shown here for the resonant photoionization of argon into the levels 23 (upper set) and 27 (lower set) as indicated in Table II. Calculations including the full treatment of all resonances (solid line) in formula (1) are compared with those including only $2p_{3/2}^5 3d J=1$ (dotted line) and $2p_{3/2}^5(3d+5s) J=1$ (dashed line); again, all computations here have been carried out for our “best” representation of the atomic bound states.

associated with the $2p_{1/2}^5 4s J=1$ or the (three) $2p_{3/2}^5(3d+5s) J=1$ resonances, respectively. From high-resolution experiments [20,38], in fact, it is known that these resonances appear very close in energy with a relative splitting of only ~ 0.4 eV. In particular, that $2p_{3/2}^5 3d$ and $2p_{3/2}^5 5s J=1$ resonances are *quasidegenerate*, if compared with their widths of about 125 meV. Therefore, all four of the resonances “overlap” with each other and may decay rapidly to one of the $3p^4(nd+n's)$ final states in the case of a spectator decay, or to any of the $3s3p^6 2S_{1/2}$ and $3s^2 3p^5 2S^+ 1L_J$ fine-structure levels, if the $3d$ or $4s, 5s$ spectator electron becomes involved into the autoionization.

To analyze the (relative) intensities and angular distributions of the photoelectrons across these four resonances, care about the wave functions has to be taken at least for the intermediate resonance states. Since the autoionization of atoms and ions depends purely on the correlated motion of the many-electron system, the quality of these wave functions finally determines how well one does understand the excitation and decay dynamics in such a unified treatment as displayed in formula (1). Taking the $2p^5 3s^2 3p^6(3d+4s)$ as the two *reference* configurations for the generation of the wavefunction expansion [30] in ansatz (5), a series of test compu-

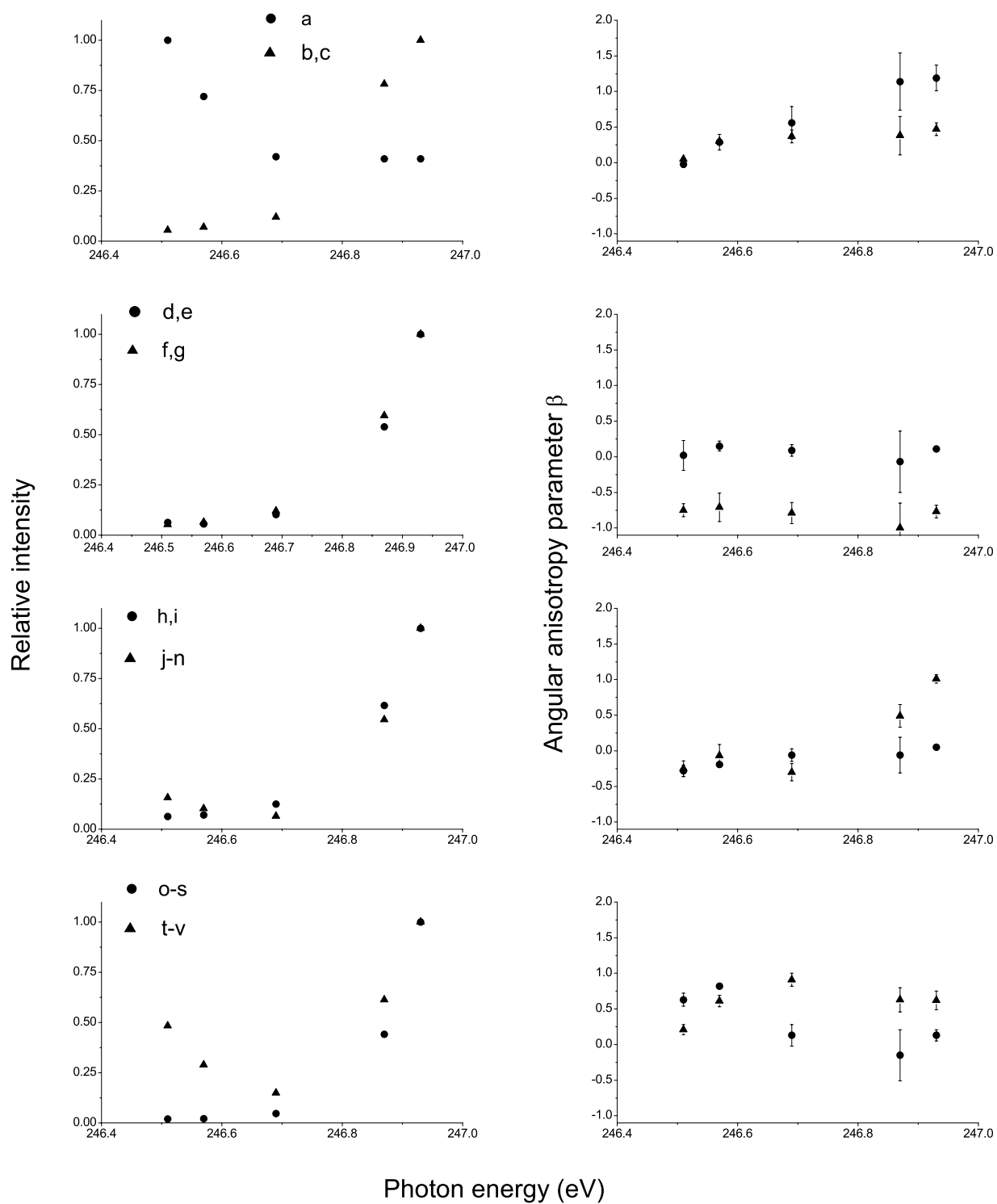


FIG. 5. Observed relative intensities (left) and angular anisotropy parameters β (right) of the photoelectrons as a function of the photon energy ($h\nu$) in the region of the $2p_{1/2}^5 4s$ and $2p_{3/2}^5 (3d+5s)$ $J=1$ resonances. Results from high-resolution measurements are shown for the resonant photoionization of argon into eight additional fine-structure levels or level groups as indicated in Fig. 1 by small letters. To facilitate the comparison with further experimental and theoretical studies, typical error bars are shown for angular parameters.

tations have first been carried out where we included all single excitations into the $4s, 3d, 5s, 4d, 6s, 5d, 7s$ subshells. This leads to a wave-function expansion with a total of 17 CSFs for the $J=1$ resonance states. Although such a limited expansion does not allow one to “monitor” the convergence

of the transition amplitudes, as involved in Eq. (1), it enables us in Fig. 2 below to compare the results from a single configuration approximation (A) with those, where virtual single excitations of the valence-shell electrons have been taken into account (approximation B). Table I displays the calcu-

lated excitation energies and width of the four $J=1$ resonances and compares them with experimental data. However, in order to facilitate the comparison, the fine-structure splitting of the intermediate resonances was adopted to the splitting measured by King *et al.* [38], while the total decay widths were taken from the experiments by Sairanen *et al.* [20].

In the last column of Table I, moreover, we display the leading LS (parent) terms in the wave-function expansion of the four resonances by transforming these functions into a LSJ -coupled basis [39]. Although these leading terms slightly depend on the approximation of the atomic resonances due to the MCDF procedure, they result from a *unitary* transformation of the standard jj - into a LSJ -coupled basis and hence, reflect the overall of the atomic levels under consideration. The decomposition in Table I shows, in particular, that these resonances are all reasonably *pure* with regard to the symmetry character of the “spectator electron.” Although these resonances strongly overlap, this “conservation” of the one-particle symmetry of the spectator electron can be well understood owing to the formation of either a $2p_{1/2}$ or $2p_{3/2}$ core hole. In general, however, the leading dynamics of the $3p^4nl$ satellite emission of argon at 246 eV is determined not only by the electronic structure of the four resonances but also by their coupling (i.e., by the moduli and phases of the autoionization amplitudes) to the final states of the Ar^+ ions.

B. Final states

The autoionization of the $2p_{1/2,3/2}^5$ hole states of argon mainly proceeds via spectator decay to one of the $3p^4(3d+4s+5s)$ final excited states with $J_f=1/2, \dots, 9/2$ but to some extent also into the $3s3p^6\ ^2S_{1/2}$ and the $3s^23p^5$ ground-state configuration of Ar^+ . For all of these (final) states of the photoion, the electron density has stabilized so far that only a photon emission may occur (except for the 1S_0 ground state). This means that these final states are stable with regard to an autoionization and hence, have negligible level widths. In the present investigation, emphasis is placed on the relative intensities and angular distributions of these emitted photoelectrons, which are associated with the $3p^4(3d+4s+5s)J_f$ spectator lines. As shown below, the population of these final states depends sensitively on the interplay of the various excitation and decay *paths* if the photon energy is varied across the resonances.

Table II displays the level classification and excitation energies of the 30 lowest levels, relative to the $3p^6\ ^1S_0$ argon ground state. In the observed electron spectrum (Fig. 1), these spectator lines therefore correspond to the lines at the low binding-energy side, labeled 1–30. In the last column of this table, we also show the leading LS parent terms in the decomposition of the wave functions with a weight of $\geq 4\%$. Note that only those $3p^4nl$ final states are reasonably pure in a LS -coupling scheme, which have angular momentum values $J_f \geq 7/2$, while the $J_f=1/2, \dots, 5/2$ fine-structure levels typically contain admixtures from several (parent) terms.

C. Photoionization via the $2p_{1/2}^54s$ $J=1$ resonance

From a simplified viewpoint, the photoexcitation and autoionization of argon occurs either via the $2p_{1/2}^54s$ or the

$2p_{3/2}^5(3d+5s)$ resonances. In this picture, the nd or $n's$ spectator electron keeps its spatial character (angular symmetry) so that the decay of any resonance always leads to a corresponding final state (configuration). In practice, however, there occurs both an overlap as well as the configuration mixing of the various resonances, which then results in the constructive or destructive interference of the corresponding amplitudes. Frankly speaking, there is an overlap of two or more Lorentz profiles (due to the individual resonances) with a relative weight as given by the energy denominators and the product of the transition amplitudes. In dependence of the energy and the relative phase of the excitation and Auger amplitudes in Eq. (1), therefore, we shall expect an interference near and across the resonances.

The $2p_{1/2}^54s$ resonance is still rather isolated at a photon energy of $\omega_{ph}=246.514$ eV; it is separated from the $2p_{3/2}^5(3d+5s)$ resonances by about 0.4 eV. In Figs. 2 and 3, the results for relative intensities and angular distribution parameters are shown for four $3p^44s$ final levels of the argon ion comparing two theoretical approximations with experiment. While approximation *A* corresponds to the calculation without any configuration mixing between the resonances or final states, approximation *B* includes the full multiconfiguration expansion for the representation of the resonances and final states. As seen clearly, the admixture of the $3p^43d$ final states leads to a rather asymmetric behavior of the β anisotropy parameters as well as to an enhancement of the relative intensity, when photon energy approaches the $2p_{3/2}^5(3d+5s)$ resonance. Although the resolution of the present experiment is high enough to resolve most of the final states in the spectra, for some lines the fine-structure splitting is so small that they cannot be resolved individually. In these cases, the observed intensities and angular distributions result from the (incoherent) summation over several final states. Figure 2 therefore shows also the *averaged* relative intensity and angular distribution for two final states. Apparently, the multiconfiguration calculations match the experimental values very well, in particular, if averaged over the two final states.

D. Photoionization via the $2p_{3/2}^5(3d+5s)$ $J=1$ resonances

The strong $2p_{3/2}^53d$ resonance at 246.927 eV is almost completely overlapped with the $2p_{3/2}^55s$ resonance. In practice, however, the excitation (absorption) strength into the $5s$ resonance is weak and only contributes about 25 percent when compared to the $2p_{3/2}^53d$ ones. For photon energies $\hbar\omega \approx 246.9$ eV, that is, near to the $2p_{3/2} \rightarrow 3d$ resonant excitation, a strong photoelectron emission is expected into those final states that have a $3d$ (spectator) electron. Figure 4 displays the relative intensities and angular distributions for two fine-structure levels with mainly a $3p^43d$ character. Here, a comparison of the highly resolved experimental data is made with MCDF calculations in three different approximations: Including all four resonances in formula (1); including the three $2p_{3/2}^5(3d+5s)$ resonances, and finally by taking only two $2p_{3/2}^53d$ resonances into account. As is seen from this figure, the relative intensity is not well predicted by our calculations for the final level 23, which contains a strong mixture of the $3p^44s$ configuration. However, the angular aniso-

TABLE III. Experimental binding energies (in eV) and LS terms of the $3p^4nl$ satellite states a–v as marked in Fig. 1, taken from Ref. [21].

Label	Final state	J_f	Energy (eV) [21]	LS term [21]
a	$3p^44p$	5/2	36.887	$4p(^1D)^2F$
b	$3p^44p$	3/2	37.112	$4p(^1D)^2P$
c	$3p^43d$	5/2	37.127	$3d(^1D)^2D$
d	$3p^43d$	3/2	37.188	$3d(^1D)^2D$
e	$3p^44p$	3/2	37.252	$4p(^1D)^2D$
f	$3p^43d$	3/2	37.384	$3d(^1D)^2P$
g	$3p^43d$	1/2	37.435	$3d(^1D)^2P$
h	$3p^43d$	5/2	38.027	$3d(^1S)^2D$
i	$3p^43d$	3/2	38.069	$3d(^1S)^2D$
j	$3p^44d$	7/2	38.534	$4d(^3P)^4D$
k	$3p^44d$	5/2	38.548	$4d(^3P)^4D$
l	$3p^44d$	3/2	38.571	$4d(^3P)^4D$
m	$3p^43d$	1/2	38.585	$3d(^1D)^2S$
n	$3p^44d$	1/2	38.597	$4d(^3P)^4D$
o	$3p^44d$	5/2	38.830	$4d(^3P)^4F$
p	$3p^44d$	1/2	38.842	$4d(^3P)^4P$
q	$3p^44d$	3/2	38.863	$4d(^3P)^4F$
r	$3p^44d$	3/2	38.879	$4d(^3P)^4P$
s	$3p^44d$	5/2	38.931	$4d(^3P)^4P$
t			40.010	
u	$3p^45s$	5/2	40.044	$5s(^1D)^2D$
v	$3p^44f$	3/2	40.070	$4f(^3P)$

tropy parameter β still agrees reasonably well for this final state indicating a quite similar behavior of involved CSFs. In contrast, good agreement is found in Fig. 4 for the relative intensity and the angular parameter of the level 27, which has mainly a $3p^43d\ ^2F_{5/2}$ character. For level 23, a clear effect is seen in the relative intensity and angular distribution parameter when the $5s$ resonance is “switching off.” For level 27, a similar effect is found in the behavior of the relative intensity but not so clearly in the angular distribution parameter due to the almost zero value of the β parameter. Note that the $2p$ hole in the electron configuration of $2p_{3/2}^54s$ and $2p_{3/2}^5(3d+5s)$ resonances has a different angular character, i.e., a different spatial distribution.

E. Further experimental data

To facilitate further theoretical studies on the resonant photoionization with excitation, Fig. 5 displays the relative intensities and angular distributions for the resonant photoexcitation into eight final states or group of states from the $3p^4(nd+n's+np)$ configurations, which often shows a quite characteristic resonance behavior. Assignments of the final levels a–v (see Fig. 1), based on the optical data, are given in Table III. The relative intensities of most of the lines increase as a function of photon energy towards the $2p_{3/2}^53d\ J=1$ resonances at 246.6, ..., 246.8 eV. This increase in the intensity therefore indicates a strong $3d$ character of the corresponding final states or group of final states. This is in line with the

assignments of the lines c, d, f, g, h, and i in optical data [21]. Groups of lines j–n and o–s seem to display quite similar behavior as the $3p^43d$ final states, which indicates strong mixing of $3p^43d$ and $3p^44d$ configurations, similar to that seen in Table II for some of the states 1–30. Line a is assigned to the final-state configuration $3p^44p$ in Ref. [21]. Its behavior, decreasing cross section, clearly deviates from what is seen for other lines. The behavior of the line v, assigned as $3p^44f$ in Ref. [21], also deviates from the general tendency. The states of negative parity are not populated via spectator decay of the $2p^5(3d+4s+5s)$ resonances in our calculations.

The angular anisotropy parameters vary slightly as a function of photon energy. The stronger variations seen in Figs. 2–4 are most probably smeared out because of averaging over several fine-structure levels.

V. SUMMARY AND CONCLUSIONS

High-resolution intensities and angular distributions of the $3p$ photoelectron of argon are presented for the $3p^6 \rightarrow 3p^4(3d+4s+5s)$ ionization with excitation across the $2p_{1/2}^54s$ and $2p_{3/2}^5(3d+5s)$ resonances. Compared with previous experiments on the $2p \rightarrow 4s$ and $2p \rightarrow 3d$ resonant Auger emission, the increase in the photon and electron resolution of the present measurements has helped reveal many details about the excitation-ionization mechanism of noble gases and about the dynamics of the atomic photoionization near to

resonances in the continuum. To analyze the intensities and angular distributions of the emitted electrons, detailed MCDF calculations have been carried out including both the direct photoionization as well as the resonant excitation with subsequent Auger emission. While the direct ionization remains negligible for all the $2p_{1/2}^5 4s$ and $2p_{3/2}^5(3d+5s)$ resonances, it is shown that a detailed understanding of the satellites of the photoelectron emission can be obtained only if the overlap of the resonances and the phases of the various “ionization paths” are taken into account. In particular, the interplay of the different resonances play an important role in the interpretation of the experimental results.

Overall, very reasonable agreement has been found between experiment and the resonant computations (outlined in Sec. II) by applying MCDF wave functions and coherent superposition of the various resonances. Some (minor) discrepancies remain for the position and the widths of the resonances as well as between the theoretical and experimental dipole parameters β . Since these experiments provide for the first time such a high resolution in the electron spectra in going across the resonances, we hope they will stimulate

further theoretical advancements including relaxation effects and an improved treatment of electronic correlations. Very likely, such improvements are necessary both for the bound-state densities with inner-shell holes and their coupling to the continuum. The latter (so-called) interchannel interactions, in particular, require a tedious principal-value integration [35]. Although the main computational steps are well understood for this part of the interaction, there is presently no implementation available that could incorporate all these effects consistently.

ACKNOWLEDGMENTS

We are grateful to the staff of the MAX synchrotron radiation laboratory for help during the measurements. Financial support from the Research Council for the Natural Sciences of the Finnish Academy and the European Community–Access to Research Infrastructure Action of the Improving Human Potential Programme are acknowledged. S.F. acknowledges support by the DFG under the project No. FR 1251/13.

-
- [1] M. O. Krause and C. D. Caldwell, in *VUV and Soft X-Ray Photoionization*, edited by U. Becker and D. A. Shirley (Plenum Press, New York-London, 1996), p. 181.
- [2] G. S. Brown, M. H. Chen, B. Crasemann, and G. E. Ice, *Phys. Rev. Lett.* **45**, 1937 (1980).
- [3] A. Kivimäki, A. Naves de Brito, S. Aksela, H. Aksela, O.-P. Sairanen, A. Ausmees, S. J. Osborne, L. B. Dantas, and S. Svensson, *Phys. Rev. Lett.* **71**, 4307 (1993).
- [4] B. G. Armen, H. Aksela, T. Åberg, and S. Aksela, *J. Phys. B* **33**, R49 (2000).
- [5] M. Meyer, E. von Raven, B. Sonntag, and J. E. Hansen, *Phys. Rev. A* **49**, 3685 (1994).
- [6] R. Camilloni, M. Žitnik, C. Comicioli, K. C. Prince, M. Zaccagna, C. Crotti, C. Ottaviani, C. Quaresima, P. Perfetti, and G. Stefani, *Phys. Rev. Lett.* **77**, 2646 (1996).
- [7] M. Alagia, L. Avaldi, M. Coreno, M. de Simone, R. Richter, S. Stranges, and M. Tabrizchi, *J. Electron Spectrosc. Relat. Phenom.* **144**, 67 (2005).
- [8] S. Alitalo, T. Matila, H. Aksela, A. Kivimäki, M. Jurvansuu, and S. Aksela, *Phys. Rev. A* **62**, 032710 (2000).
- [9] R. R. T. Marinho, O. Björneholm, S. L. Sorensen, I. Hjelte, S. Sundin, M. Bässler, S. Svensson, and A. Naves de Brito, *Phys. Rev. A* **63**, 032514 (2001).
- [10] B. Obst, J. E. Hansen, B. Sonntag, Ph. Wernet, and P. Zimmermann, *Phys. Rev. A* **65**, 062716 (2002).
- [11] B. M. Lagutin, I. D. Petrov, V. L. Sukhorukov, S. Kammer, S. Mickat, R. Schill, K. H. Scharfner, A. Ehresmann, Y. A. Shutoy, and H. Schmoranzner, *Phys. Rev. Lett.* **90**, 073001 (2003).
- [12] M. Meyer, A. Marquette, A. N. Grum-Grzhimailo, U. Kleiman, and B. Lohmann, *Phys. Rev. A* **64**, 022703 (2001).
- [13] M. Kitajima, M. Okamoto, Y. Shimizu, H. Chiba, S. Fritzsche, N. M. Kabachnik, I. P. Sazhina, F. Koike, T. Hayaishi, H. Tanaka, Y. Sato, and K. Ueda, *J. Phys. B* **34**, 3829 (2001); K. Ueda, M. Kitajima, A. De Fanis, Y. Tamenori, H. Yamaoka, H. Shindo, T. Furuta, T. Tanaka, H. Tanaka, H. Yoshida, R. Sankari, S. Aksela, S. Fritzsche, and N. M. Kabachnik, *Phys. Rev. Lett.* **90**, 153005 (2003).
- [14] P. O’Keeffe, S. Aloise, S. Fritzsche, B. Lohmann, U. Kleiman, M. Meyer, and A. N. Grum-Grzhimailo, *Phys. Rev. A* **70**, 012705 (2004).
- [15] S. Ricz, J. Nikkinen, R. Sankari, T. Ricsóka, Á. Kövér, D. Varga, S. Fritzsche, H. Aksela, and S. Aksela, *Phys. Rev. A* **72**, 014701 (2005).
- [16] M. Bässler, J.-O. Forsell, O. Björneholm, R. Feifel, M. Jurvansuu, S. Aksela, S. Sundin, S. L. Sorensen, R. Nyholm, A. Ausmees, and S. Svensson, *J. Electron Spectrosc. Relat. Phenom.* **101-103**, 953 (1999).
- [17] M. Bässler, A. Ausmees, M. Jurvansuu, R. Feifel, J.-O. Forsell, P. de Tarso Fonseca, A. Kivimäki, S. Sundin, S. L. Sorensen, R. Nyholm, O. Björneholm, S. Aksela, and S. Svensson, *Nucl. Instrum. Methods Phys. Res. A* **469**, 382 (2001).
- [18] R. Nyholm, S. Svensson, J. Nordgren, and A. Flodström, *Nucl. Instrum. Methods Phys. Res. A* **246**, 267 (1986).
- [19] S. Aksela, A. Kivimäki, R. Nyholm, and S. Svensson, *Rev. Sci. Instrum.* **63**, 1252 (1992).
- [20] O.-P. Sairanen, A. Kivimäki, E. Nömmiste, H. Aksela, and S. Aksela, *Phys. Rev. A* **54**, 2834 (1996).
- [21] C. E. Moore, *Ionization Potentials and Ionization Limits Derived from the Analysis of Optical Spectra* (U.S. GPO, Washington, D.C., 1970); C. E. Moore, *Ionization Potentials and Ionization Limits Derived from the Analysis of Optical Spectra*, Vol. 1 (US GPO, Washington, D.C., reissued 1971).
- [22] H. Aksela and J. Mursu, *Phys. Rev. A* **54**, 2882 (1996).
- [23] J. Mursu, H. Aksela, O.-P. Sairanen, A. Kivimäki, E. Nömmiste, A. Ausmees, S. Svensson, and S. Aksela, *J. Phys. B* **29**, 4387 (1996).
- [24] K. Ueda, Y. Shimizu, H. Chiba, M. Kitajima, H. Tanaka, S. Fritzsche, and N. M. Kabachnik, *J. Phys. B* **34**, 107 (2001).

- [25] K. Ueda, Y. Shimizu, H. Chiba, M. Kitajima, M. Okamoto, M. Hoshino, H. Tanaka, T. Hayashi, S. Fritzsche, I. P. Sazhina, and N. M. Kabachnik, *J. Phys. B* **36**, 319 (2003).
- [26] S. Fritzsche, A. Surzhykov, and T. Stöhlker, *Phys. Rev. A* **72**, 012704 (2005).
- [27] S. Baier, A. N. Grum-Grzhimailo and N. M. Kabachnik, *J. Phys. B* **27**, 3363 (1994).
- [28] I. P. Grant, in *Methods in Computational Chemistry*, edited by S. Wilson (Plenum Press, New York, 1988), Vol. 2, p. 1.
- [29] S. Fritzsche, *Phys. Scr., T* **T100**, 37 (2002).
- [30] F. A. Parpia, C. Froese Fischer, and I. P. Grant, *Comput. Phys. Commun.* **94**, 249 (1996).
- [31] S. Fritzsche, *J. Electron Spectrosc. Relat. Phenom.* **114-116**, 1155 (2001).
- [32] S. Fritzsche, H. Aksela, C. Z. Dong, S. Heinäsmäki, and J. E. Sienkiewicz, *Nucl. Instrum. Methods Phys. Res. B* **205**, 93 (2003).
- [33] M. Kutzner and V. Radojevic, *Phys. Rev. A* **49**, 2574 (1994).
- [34] S. Fritzsche, C. Froese Fischer, and C. Z. Dong, *Comput. Phys. Commun.* **124**, 340 (2000).
- [35] S. Fritzsche, B. Fricke, and W.-D. Sepp, *Phys. Rev. A* **45**, 1465 (1992); S. Fritzsche, *Phys. Lett. A* **180**, 262 (1993).
- [36] J. Tulkki, N. M. Kabachnik, and H. Aksela, *Phys. Rev. A* **48**, 1277 (1993).
- [37] S. Fritzsche, G. Zschornack, G. Musiol, and G. Soff, *Phys. Rev. A* **44**, 388 (1991).
- [38] G. C. King, M. Tronc, F. H. Read, and R. C. Bradford, *J. Phys. B* **10**, 2479 (1977).
- [39] G. Gaigalas, T. Zalandauskas, and S. Fritzsche, *Comput. Phys. Commun.* **157**, 239 (2004).